

1 **Title:**

2 Climate, CO₂, and human population impacts on global wildfire emissions

3 **Authors:**

4 W. Knorr*¹, L. Jiang & A. Arneth³

5 ¹Physical Geography and Ecosystem Analysis, Lund University, Sölvegatan 12,
6 22362 Lund, Sweden

7 ²National Center for Atmospheric Research, Boulder, Colorado, USA

8 ³KIT/IMK-IFU, Garmisch-Partenkirchen, Germany

9 *Corresponding author's email: wolfgang.knorr@nateko.lu.se

10

11 **Abstract:**

12 Wildfires are by far the largest contributor to global biomass burning and constitute a
13 large global source of atmospheric traces gases and aerosols. Such emissions have a
14 considerable impact on air quality and constitute a major health hazard. Biomass
15 burning also influences the radiative balance of the atmosphere and is thus not only of
16 societal, but also of significant scientific interest. There is a common perception that
17 climate change will lead to an increase in emissions as hot and dry weather events that
18 promote wildfire will become more common. However, even though a few studies
19 have found that the inclusion of CO₂ fertilization of photosynthesis and changes in
20 human population patterns will tend to somewhat lower predictions of future wildfire
21 emissions, no such study has included full ensemble ranges of both climate
22 predictions and population projections, including the effect of different degrees of
23 urbanisation.

24 Here, we present a series of 124 simulations with the LPJ-GUESS-SIMFIRE global
25 dynamic vegetation – wildfire model, including a semi-empirical formulation for the

26 prediction of burned area based on fire weather, fuel continuity and human population
27 density. The simulations comprise Climate Model Intercomparison Project 5 (CMIP5)
28 climate predictions from eight Earth System Models using two Representative
29 Concentration Pathways and five scenarios of future human population density based
30 on the series of Shared Socioeconomic Pathways (SSPs), sensitivity tests for the
31 effect of climate and CO₂, as well as a sensitivity analysis using two alternative
32 parameterisations of the semi-empirical burned-area model. Contrary to previous
33 work, we find no clear future trend of global wildfire emissions for the moderate
34 emissions and climate change scenario based on the Representative Concentration
35 Pathway (RCP) 4.5. Only historical population change introduces a decline by around
36 15% since 1900. Future emissions could either increase for low population growth
37 and fast urbanisation, or continue to decline for high population growth and slow
38 urbanisation. Only for high future climate change (RCP8.5), wildfire emissions start
39 to rise again after ca. 2020 but are unlikely to reach the levels of 1900 by the end of
40 the 21st century. We find that climate warming will generally increase the risk of fire,
41 but that this is only one of several equally important factors driving future levels of
42 wildfire emissions, which include population change, CO₂ fertilisation causing woody
43 thickening, increased productivity and fuel load, and faster litter turnover in a warmer
44 climate.

45

46 **1 Introduction**

47 Wildfires are responsible for approximately 70% of the global biomass burned
48 annually (van der Werf et al. 2010, updated). Emissions from wildfires in the form of
49 trace gases and aerosols can have a considerable impact on the radiative balance of
50 the atmosphere (Langmann et al. 2009) and also constitute a large source of
51 atmospheric pollutants (Kasischke and Penner 2004). At the same time, wildland fires
52 are an important component of terrestrial ecosystems (Bowman et al. 2009) and the
53 Earth system in (Arnell et al. 2010). Fires respond to changes in climate, vegetation
54 composition and human activities (Krawchuk et al. 2009, Pechony and Shindell 2010,
55 Kloster et al. 2012, Moritz et al. 2012), with some model simulations showing a
56 positive impact of climate change on emissions during the 21st century, but a negative,
57 albeit smaller, impact due to changes in land use and increased fire suppression
58 (Kloster et al. 2012).

59 Empirical studies designed at isolating the effect of human population density – here
60 used as an aggregate value representing human interference at the landscape scale –
61 have generally shown that higher population density *per se* leads to a decrease in the
62 annual area burned (Archibald et al. 2008; Knorr et al. 2014; Bistinas et al. 2014),
63 even though there is a common perception that wildfire activity peaks at intermediate
64 levels of population density. This apparent paradox was shown to be the result of co-
65 variations between population density and other factors such as fuel load or
66 flammability - if these co-variations are taken into account, the view of a negative
67 impact is consistent with the observed peak (Bistinas et al. 2014).

68 The main future drivers of changing wildfire have potentially opposing effects on
69 emissions – temperature (increasing), CO₂ via productivity (increasing), CO₂ via
70 woody thickening (Wigley et al., 2010; Buitenwerf et al. 2012; decreasing), and

71 human population density (decreasing emissions). In the meantime, socio-
72 demographic change, interacting with other economic and technological factors, may
73 also lead to climate change – e.g. slow population growth combined with a
74 conventional development pathway of high fossil fuel dependence would result in
75 high CO₂ emissions and large temperature increases. Moreover, the same population
76 growth but with different urbanization trends could also lead to different levels of
77 spatial population distributions and concentrations, and consequently different results
78 concerning wildfire emissions. Therefore, it is important to first assess the impact of
79 each factor individually before arriving at conclusions concerning aggregate effects.
80 Another important point of consideration is that if climate forcing is based on a model
81 with low climate sensitivity to CO₂ change (i.e. relatively small change in global
82 mean temperature simulated for a given rise in atmospheric CO₂), CO₂ effects might
83 dominate over climate effects. The reverse applies to climate models with a high
84 climate sensitivity. We therefore use an ensemble of climate models instead of only
85 one or two, consider a wide range of future scenarios of population density change,
86 and differentiate between the effects of changes in not only population sizes within a
87 country, but also population spatial distribution via urbanisation.

88 While previous studies have focused on the task of predicting future wildfire
89 emissions and have at most considered impacts of population changes separately to
90 those of climate and CO₂, here we partition the projected changes into the following
91 drivers: climate via changes in burned area, climate via changes in fuel load, CO₂ via
92 changes in burned area, CO₂ via changes in fuel load, and population density
93 considering both the effects of population growth and urbanisation. The goal is a
94 better understanding of the underlying processes of wildfire emission changes, which
95 should help establishing the necessary links between climate policy (emissions),

96 climate science (climate sensitivity), demography, air pollution and atmospheric
97 chemistry, as well as wildfire management.

98 **2 Methods**

99 *2.1 Models and driving data*

100 We use the coupled fire-vegetation model LPJ-GUESS-SIMFIRE (Knorr et al. 2014;
101 Knorr et al. submitted) to simulate establishment, growth and mortality of natural
102 vegetation, fuel load, burned area and wildfire emissions under changing climate, CO₂
103 and human population density. LPJ-GUESS (Smith et al. 2001) is a global dynamic
104 vegetation model that simulates potential vegetation as a mixture of user-defined plant
105 functional types (PFTs) which compete with each other in so-called patches. Each
106 PFT is characterized by a set of traits, such as leaf longevity and phenology, growth
107 form and bioclimatic limits to establishment and survival. In these simulations, we use
108 five patches per grid cell, and within each patch, LPJ-GUESS simulates several age
109 cohorts. In "cohort mode", which is used here, all individuals of a cohort are assumed
110 to have identical characteristics. When a fire occurs, individuals of woody PFTs
111 within each patch a selected at random to be killed or to survive according to the
112 PFT's fire resistance (Knorr et al. 2012). Grass PFTs have no individuals and
113 therefore we only adjust the biomass of each these PFTs. We use PFTs designed for
114 global simulations as given by Ahlström et al. (2012).

115 Fire impacts on vegetation are simulated at monthly intervals as described by Knorr et
116 al. (2012). SIMFIRE predicts annual fractional burned area, A (the fraction of each
117 grid cell burned per year) using the following equation:

$$118 \quad A(y) = a(B) F^b N_{max}(y)^c \exp(-ep) \quad (1)$$

119 Here, y is the fire year defined as in Knorr et al. (2012) in such a way that it never
 120 "cuts" the fire season into two, B the biome type, F is annual potential fraction of
 121 absorbed photosynthetically active radiation (FAPAR), an approximation of
 122 vegetation fractional cover easily observed from satellites and here used as a measure
 123 of fuel continuity (Knorr et al. 2014), N_{max} is the annual maximum Nesterov Index
 124 based on daily diurnal temperature mean, T_m , range, T_r , and precipitation, P , and p is
 125 human population density. The Nesterov index used is given by Thonicke et al.
 126 (2010) as the cumulative sum of $T_m*(T_r + 4K)$ over all consecutive days with equal or
 127 less than 3 mm rainfall. $a(B)$, b , c , and e are global parameters derived by
 128 optimisation of SIMFIRE burned area against observed burned area from GFED3
 129 (Giglio et al. 2010) on a spatial grid and for the entire globe (Table 2, "GFED3", "All
 130 population densities" of Knorr et al. 2014). To derive monthly burned area, we use
 131 the average diurnal cycle of burned area derived from GFED3 for 2001-2010 using a
 132 variable spatial averaging radius around each grid cell which is at least 250km but has
 133 a total burned area over the period of 10,000km². Information on biome type is passed
 134 from LPJ-GUESS to SIMFIRE, where biome type is a discrete number ranging from
 135 one to eight, using FAPAR of woody and herbaceous vegetation and of vegetation of
 136 at least 2m as well as geographic latitude as information. F in Eq. (1) is a bias
 137 corrected value derived from LPJ-GUESS simulated FAPAR, F_s , via:

$$138 \quad F = 0.42 F_s - 0.15 F_s^2 \quad (2)$$

139 In LPJ-GUESS, woody thickening effects emissions in two ways: When the fraction
 140 of shrubs increases, the area belonging to the biome "shrubland" increases relative to
 141 the area of the biome "savannah and grassland". Because $a(B)$ of Eq.(1) for the
 142 former is approximately half of the value for the latter (Knorr et al. 2014), an
 143 increase in the fraction of shrubland immediately leads to a decrease in burned area.

144 The second effect results from the fact that in a fire, 100% of live and dead leaves of
145 grasses burn, while for woody vegetation, 100% of dead leaves but only between 46
146 and 59% of live leaves (depending on fire resistance), 20% of dead wood and no live
147 wood burn in a fire (Knorr et al. 2012). As a result, the fraction of net primary
148 productivity emitted in a fire tends to decrease with woody encroachment. The
149 measure used to document woody thickening in LPJ-GUESS is the maximum
150 seasonal leaf area index (LAI) assigned the woody individuals of a grid cell divided
151 by the total grid cell LAI.

152 LPJ-GUESS-SIMFIRE, in the following denoted "LPJ-GUESS", is driven by output
153 from Earth system model (ESM) simulations from the CMIP5 project (Taylor et al.
154 2012) in a way mostly following Ahlström et al. (2012), where climate output of
155 monthly mean temperature, precipitation and downward shortwave radiation is bias
156 corrected using the mean observed climate for the period 1961-1990, and atmospheric
157 CO₂ levels used by LPJ-GUESS are taken from the RCP scenarios as prescribed for
158 CMIP5 (Meinshausen et al. 2011). In variance to the cited work, we use CRU TS3.10
159 (Harris et al. 2014) as climate observations, and we predict monthly mean diurnal
160 temperature range and number of wet days per month based on linear regressions
161 against mean temperature and precipitation, respectively. Simulations are carried out
162 on an equal-area pseudo-1° grid, which has a grid spacing of 1°x1° at the equator and
163 a wider E-W spacing towards the poles in order to conserve the average grid cell area
164 per latitude band.

165 We use global historical gridded values of human population density from HYDE
166 (Klein-Goldewijk et al. 2010) for simulations up to 2005. For future scenarios, no
167 gridded data are available, but we use instead per-country values of total population
168 and percentage of urban population. In order to generate gridded population density

169 after 2005, we use separate urban and rural population density from HYDE for the
170 year 2005 and re-scale both by the relative growth of each in each country. After this
171 procedure, we multiply the population density of all grid cells representing each
172 country by a constant factor such that the growth of the total population of the given
173 country relative to the 2005 HYDE data matches that of the per-country total
174 population scenario used.

175 ***2.2 Scenarios***

176 We run simulations for two climate change scenarios from the Representative
177 Concentration Pathways (RCP). Of these, RCP4.5 represents an approximate radiative
178 forcing scenario typical of the majority of stabilization scenarios included in the
179 Fourth Assessment of Report of the International Panel on Climate Change. The
180 other, RCP8.5, is a typical case of high emissions resulting from a lack of enforced
181 stabilization of greenhouse gases, leading to high levels of climate change (van
182 Vuuren et al. 2011). In this study, we will consider both scenarios separately as two
183 alternative futures without any assignment of relative probabilities.

184 Climatic trends simulated for the 20th century as well as for RCP4.5 and RCP8.5 are
185 shown in Table 1 for different regions, for the eight-ESM ensemble mean and range.
186 (For definition of regions see Section 2.4 and Fig. 4.) There is a spatially rather
187 uniform warming trend of around half a °C during the 20th century roughly in
188 accordance with observations (Harris et al. 2014), with inter-model differences larger
189 than differences between regions. Precipitation declines slightly during the same
190 period, most strongly for already dry Middle East, with generally rather large inter-
191 model differences, in particular for Africa, Oceania and South Asia. Temperature
192 change under the RCP4.5 scenario towards the end of the 21st century is around

193 +2.5°C for most regions, except for higher values for the two regions comprising most
194 of the Arctic (North America, North Asia), while precipitation overall increases, albeit
195 with considerable declines for Oceania and Middle East on average, and for South
196 America and Africa for their respective ensemble minima. For RCP8.5, global
197 mean temperature change reaches as high as +5°C, with North America, North Asia
198 and Middle East exceeding this value. Precipitation changes are similar to RCP4.5,
199 but with both the inter-model ranges and the inter-region differences considerably
200 amplified. (For example, there is an almost 40% decline for Oceania for the ensemble
201 minimum.)

202 For population scenarios, we use marker scenarios of the Shared Socioeconomic
203 Pathways (SSPs; O'Neill et al. 2012, Jiang 2014). Following Knorr et al. (submitted),
204 we consider a total of five scenarios: SSP2 scenario with medium population growth
205 and central urbanisation, two extreme scenarios with either high population growth
206 and slow urbanisation (SSP3) or low population growth with fast urbanisation (SSP5),
207 and two further scenarios in which the medium population growth (SSP2) is
208 combined with either slow (SSP3) or fast (SSP5) urbanisation. For the purpose of
209 analysis, we will consider these five scenarios equally plausible, keeping in mind,
210 however, that this is mainly a working hypothesis.

211 ***2.3 Simulations***

212 We combine output from eight ESMs with two different emissions pathways, one
213 based on RCP4.5 and one on RCP8.5, all run with the medium population and central
214 urbanisation scenario of SSP2. These 16 simulations are repeated six times using the
215 other four population and urbanisation scenarios, one simulation each where
216 population is held constant at 2000 levels, and one simulation where both population
217 and atmospheric CO₂ levels are held constant at 2000 levels, giving $8 * 2 * 7 = 112$

218 simulations. To these we add two more sets of six simulations each with a different
219 parameterisation of SIMFIRE, comprising runs using the SSP2 demographic scenario,
220 fixed population, and fixed population and CO₂ and output from MPI-ESM-LR based
221 on either RCP4.5 or RCP8.5. The first alternative SIMFIRE parameterisation is
222 derived from a global optimisation against MCD45 burned area (Roy et al. 2008)
223 according to Knorr et al. (2014, Table 2, "MCD45", "All population densities"), and
224 the other assumes a slight increase in burned area with increasing population density
225 if p is less than 0.1 inhabitants per km², where Eq. (1) is replaced by:

$$226 \quad A(y) = (0.81 + 1.9p) a(B) F^b N_{max}(y)^c \exp(-ep), \quad (3)$$

227 based on results presented by Knorr et al. (2014).

228 ***2.4 Analytical Framework***

229 Since the present analysis only considers wildfires, we exclude all grid cells that
230 contain more than 50% of cropland at any time during 1901-2100 in either the
231 RCP6.0 or 8.5 land use scenarios (Hurtt et al. 2011). The threshold of 50% is the same
232 as used during SIMFIRE optimisation. A time-invariant crop mask is used in order to
233 avoid introducing time trends in the results through temporal variations of the crop
234 mask. We therefore only consider the indirect effect of cropland expansion via the
235 empirically derived burned area--population density relationship of SIMFIRE, not the
236 direct displacement of wildlands. This indirect effect can be considerable and arises
237 from the fact that cropland expansion tends to be accompanied by higher population
238 density, a denser road network, and a decrease in burned area in the areas that have
239 not been converted to croplands (Andela and van der Werf 2014).

240 The changes in emissions may be caused by climate change alone, by changes in
241 atmospheric CO₂, or by changes in population density. Emissions are determined by

242 the product of burned area, the amount of fuel present, and the fraction of fuel
 243 combusted in a fire. Climate affects burned area directly by changing fire risk via
 244 N_{max} , while climate and CO₂ effect burned area indirectly by changing the vegetation
 245 type, which affects $a(B)$, or vegetation cover, which affects F in Eq. (1). Fuel load is
 246 also affected by vegetation productivity which is driven by both climate and CO₂, and
 247 by litter decay rates, which depend on temperature and precipitation (Smith et al.
 248 2001). The combusted fraction of fuel mainly depends on the presence of grasses vs.
 249 trees (Knorr et al. 2012). Finally, population density affects emissions through burned
 250 area via Eq. (1).

251 In order to assess the effect of different driving factors on changing emissions, we
 252 employ the following analytical framework:

$$253 \quad E_{T2} = E_{T1} + \Delta E, \quad (4a)$$

$$254 \quad E_{T2}^{p2} = E_{T1}^{p2} + \Delta E^{p2}, \quad (4c)$$

$$255 \quad E_{T2}^{cp2} = E_{T2}^{cp2} + \Delta E^{cp2} \quad (4b)$$

256 with

$$257 \quad \Delta E = \Delta E_{\text{clim}} + \Delta E_{\text{CO}_2} + \Delta E_{\text{pop}}, \quad (5a)$$

$$258 \quad \Delta E^{p2} = \Delta E_{\text{clim}} + \Delta E_{\text{CO}_2}, \quad (5b)$$

$$259 \quad \Delta E^{cp2} = \Delta E_{\text{clim}}. \quad (5b)$$

260 where subscript $T1$ denotes the temporal average over the initial reference period
 261 (either 1901-1930 or 1971-2000), and $T2$ over the subsequent reference period (1971-
 262 2000 or 2071-2100), E are wildfire emissions, ΔE the change in the temporal average
 263 of emissions between the two reference periods, and the subscripts "clim", "CO₂" and
 264 "pop" denote the effects of changing climate, CO₂ and human population density. The
 265 superscripts $p2$ are for the simulations with population density fixed at year 2000

266 levels, and $cp2$ for the simulations with both CO₂ and population fixed at 2000 levels.
267 We chose the year 2000 as a reference year for fixed input variables in the middle of
268 the simulation period in order to minimise deviations from the values of the transient
269 runs.

270 The climate effect in the context of this study is therefore defined as the change in
271 emissions between two time periods of a transient simulation with variable climate
272 but fixed population density and atmospheric CO₂, the CO₂ effect as the additional
273 change in emissions when CO₂ is also varied in time, and the population effect as the
274 additional effect when population density also becomes time variant. The computed
275 effects are not expressions of model sensitivity to small perturbations, but rather arise
276 from a series of specific scenarios. We choose this order of scenarios for historical
277 reasons: we first include the effect studied most (e.g. Krawchuk et al., 2009; Moritz et
278 al., 2012), then the effect that is usually included as soon as a dynamic vegetation
279 model is used (Scholze et al. 2006), and at last the effect that is the focus of the
280 current study. If we were to add the population effect first -- by including simulations
281 where population changes in time but CO₂ is kept constant -- the results would be
282 somewhat different, and the difference could be expressed as interaction terms
283 following Stein and Alpert (1993). However, this method is usually applied to time
284 slice experiments (e.g. Claussen et al. 2001; Martin Calvo and Prentice 2015) and its
285 application to transient simulations is less straightforward, still depends on a finite
286 perturbations, and would require a large number of additional simulations, which is
287 why we here restricted ourselves to the setup described by Eqs.~(4) and (5).

288 Fire emissions here are computed as the product of burned area and area-specific fuel
289 combustion. Therefore, we can further subdivide the CO₂ effect on emissions between
290 those that work via changing burned area ($\Delta E_{CO_2}^{b,a}$) and those via changing fuel load

291 as the remainder ($\Delta E_{\text{CO}_2}^{\text{c.f.l.}} = \Delta E_{\text{CO}_2} - \Delta E_{\text{CO}_2}^{\text{b.a.}}$). We derive the former in a first-order
 292 forward projection using emissions per area burned of the previous time step::

$$293 \quad \Delta E_{\text{CO}_2}^{\text{b.a.}} = \Delta B_{\text{CO}_2} (E_{T1} / B_{T1}), \quad (6)$$

294 where B_{T1} is the temporal average of burned area during reference period $T1$, and
 295 ΔB_{CO_2} the change in burned area due to CO_2 changes, which we approximate in an
 296 analogous way to ΔE_{CO_2} as:

$$297 \quad \Delta B_{\text{CO}_2} = B_{T2}^{p2} - B_{T1}^{p2} - (B_{T2}^{cp2} - B_{T1}^{cp2}). \quad (7)$$

298 An analogous formulation is used in order to discern climate impacts due to burned
 299 area from those due to changes in fuel load and its degree of combustion:

$$300 \quad \Delta E_{\text{clim}}^{\text{b.a.}} = \Delta B_{\text{clim}} (E_{T1} / B_{T1}), \quad (8)$$

301 with

$$302 \quad \Delta B_{\text{clim}} = B_{T2}^{cp2} - B_{T1}^{cp2}. \quad (9)$$

303 We analyse the main driving factors of emissions changes using Eq. 5–9 for selected
 304 large regions, aggregated from the standard GFED regions (Giglio et al. 2010):

- 305 1. North America (GFED Boreal and Temperate North America, Central
 306 America)
- 307 2. South America (GFED Northern and Southern-Hemisphere South America)
- 308 3. Europe (same as GFED)
- 309 4. Middle East (same as GFED)
- 310 5. Africa (GFED Northern and Southern-Hemisphere Africa)
- 311 6. North Asia (GFED Boreal and Central Asia)
- 312 7. South Asia (GFED South-East and Equatorial Asia)
- 313 8. Oceania (GFED Australia and New Zealand)

314 For a probabilistic analysis of changes in emissions, we follow previous work by
315 Scholze et al. (2006), who counted ensemble members driven by differing climate
316 models where the change of the temporal average between two reference periods was
317 more than one standard deviation of the interannual variability of the first reference
318 period. The authors found a general pattern of increasing fractional burned area in arid
319 regions, and a decline at high latitudes and some tropical regions. Here, we apply the
320 method to emissions and use two standard deviations instead in order to ensure that
321 the change is highly significant.

322 **3 Results**

323 *3.1 Global emission trends*

324 Global simulated emissions taking into account changes in all factors, climate, CO₂
325 and population, decline continuously between about 1930 and 2020 for all members
326 of the ESM ensemble (Fig. 1). Thereafter, emissions approximately stabilize, albeit
327 with a very slight upward trend during 2080-2100 for the moderate greenhouse gas
328 concentrations and climate change scenario RCP4.5 and the central demographic
329 scenario (Fig. 1a). However, different demographic scenarios lead to considerable
330 variations in simulated emissions: while emissions continue to decline until 2100
331 under high population growth and slow urbanisation (SSP3), the trend of declining
332 emissions is reversed from around 2010 and the total will resume current levels by the
333 end of the 21st century under low population growth and fast urbanisation (SSP5)
334 when taking the ESM ensemble mean. In general, higher population growth drives
335 emissions downward (comparing SSP3 to SSP5), while faster urbanisation contributes
336 to higher wildfire emissions (comparing SSP2 population with fast and slow
337 urbanisation). By the end of the century, different demographic trends generate
338 approximate 0.2 GtC per year difference (ranging from around 1.1 to 1.3 GtC/yr)

339 under the moderate climate change RCP4.5. Overall, the range of future emissions
340 spanned by the eight ESMs, but using a single, central population scenario, is less
341 than half of the range spanned by all ESMs and population scenarios combined. None
342 of the simulations has late 21st century emissions reach again the levels present at the
343 beginning of the 20th century (Table 2). Only 9 out of 40 simulations show global
344 average emissions during 2071-2100 higher than during 1971-2000, seven out of
345 which are for low population growth and fast urbanisation, and one for intermediate
346 population growth and fast urbanisation.

347 Under RCP 8.5, with high greenhouse gas concentrations and climate change, global
348 wildfire emissions start to rise again after 2020 even for the central demographic
349 scenarios (SSP2) and by the end of the 21st century reach levels only slightly below
350 those of the beginning of the 20th century (Fig. 1b). According to this climate change
351 scenario, the world is currently in a temporary minimum of wildfire emissions,
352 independent of demographic scenario or ESM simulation. The population scenario
353 rather determines when emissions are predicted to rise again and how fast emissions
354 increase. For a scenario of high population growth and slow urbanisation (SSP3),
355 emissions rise again after ca. 2070 and reach about 1.2 GtC/yr by the end of the
356 century, while under the fast urbanisation scenarios (SSP5 and SSP2 population with
357 fast urbanisation), they already start rising around 2020. Under RCP8.5, different
358 demographic trends result in different wildfire emissions ranging from 1.2 to 1.5
359 GtC/yr. Overall, for 28 out of 40 simulations average emissions during 2071-2100 are
360 higher than during 1971-2000, and for three out of the eight simulations with low
361 population growth and fast urbanisation they are even higher than for 1901-1930
362 (Table 2).

363 Simulations with atmospheric CO₂ and population held constant at 2000 levels reveal
364 the impact of climate change on simulated wildfire emissions (Fig. 2a). The climate
365 impact is here shown as the difference in emissions against the average during 1971-
366 2000 (1.28 PgC/yr, see Table 2). There is a modest positive climate impact on global
367 emissions for RCP8.5, which reaches close to 10% towards the end of the 21st century
368 for the ESM ensemble mean, with a range between close to 0 and +20%. For the past,
369 there is no discernable impact of climate change. For RCP4.5, the impact is very
370 small and peaks around 2050 for the ensemble mean, but with a range skewed slightly
371 towards increased emissions.

372 The CO₂ impact is computed as the difference between two simulations with fixed
373 population density, the one with variable climate and CO₂ minus the one with variable
374 climate but fixed CO₂ (Eq. 5). The resulting emissions differences (Fig. 2b) remain
375 negative throughout the historical period until 2005 because the fixed-CO₂
376 simulations start out with considerably higher CO₂ levels than the variable-CO₂ ones
377 leading to higher productivity (CO₂ fertilisation, see Hickler et al. 2008, Ahlström et
378 al. 2012), higher fuel load and therefore higher emissions. For RCP8.5, the global
379 CO₂ impact on emissions is about the same as the climate impact, but for RCP4.5 it is
380 much larger. The magnitude of the CO₂ effect itself is climate dependent, which can
381 be seen by the inter-ensemble range, which is caused solely by differences in climate.
382 (All ensemble members use the same atmospheric CO₂ scenarios for a given RCP.)

383 There is also a small interannual variability caused mainly by climate fluctuations,
384 since interannual variations in atmospheric CO₂ are small until 2005 and absent from
385 the scenarios (Meinshausen et al. 2011). As for climate, there is no discernable CO₂
386 impact on past emission changes.

387 Finally, the demographic impact is simulated by the difference between simulations
388 with time varying climate, CO₂ and population, and the corresponding simulations
389 where population is fixed, but the other two vary with time (Eq. 5). As one would
390 expect, the results for the two RCPs are indistinguishable, with a small climate-related
391 ensemble range and a small amount of interannual variability caused by climate
392 fluctuations (Fig. 2c). The simulated demographic impact for the central population
393 scenario is towards declining emissions mainly driven by population growth. After
394 2050, the effect declines rapidly, and there is a very slight positive trend after ca. 2090
395 which is due to the leveling off of projected population growth (SSP2) and continuing
396 urbanisation. As can be seen by comparing simulated emissions between the central
397 (SSP2) and the remaining population scenarios (Fig. 1a), the demographic impact
398 varies considerably between scenarios, with a continuing negative impact until 2100
399 for the scenario with high population growth with slow urbanisation (SSP3), but a
400 positive impact of the demographic change on global emission trends from about
401 2040 for low population growth with fast urbanisation (SSP5).

402 Results for the set of sensitivity tests where the parameterisation of SIMFIRE was
403 modified are shown in Fig. 3 for the climate, CO₂ and demographic impacts
404 separately. Note that in this case, simulations are performed with only one ESM
405 (MPI-ESM-LR). The climate impact on emissions is again small for RCP4.5, but
406 discernably positive for RCP8.5 after ca. 2020. The climate impact is hardly affected
407 by changing the SIMFIRE parameterisation. The CO₂ effect is similar to the ensemble
408 mean (Fig. 2b), but with a marked decline after ca. 2080 for RCP8.5. In this case,
409 SIMFIRE optimised against MCD45 burned area shows less of a positive trend after
410 2020 as a result of CO₂ changes than the standard formulation, and a more
411 pronounced negative effect after 2080. Also, the simulated historical and future

412 demographic impacts are slightly less for MCD45 than for the standard version. The
413 SIMFIRE version with an initial increase in burned area with population density (Eq.
414 3) has only a very small impact on simulated global emissions.

415 The recent estimate from the GFED4.0s data set puts the average global wildfire
416 emissions at 1.5 PgC/yr (released May 2015, 1997-2014 average of savannah, boreal
417 and temperate forest fires combined, against 2.2 PgC/yr for all biomass burning, van
418 der Werf et al. 2010, updated using Randerson et al. 2012 and Giglio et al. 2013),
419 slightly higher than simulated here (Table 2). During the 20th century, global
420 emissions decrease by around 150 TgC/yr, a little more than 10%. The main driving
421 factor of this decrease is growing population, while climate and CO₂ changes have
422 only a very small impact on emissions, as already discussed with Fig. 2. Further
423 analysis of these driving factors (Fig. 4), however, reveals that this small impact is
424 due to compensating action on either burned area (Eqs. 6 and 8) or combustible fuel
425 load (the remainder). Globally, climate had a small positive and CO₂ a slightly
426 smaller negative effect on emissions via burned area. At the same time, climate had a
427 negative and CO₂ a positive impact on combustible fuel load. For the 21st century
428 (Fig. 5), this constellation is predicted to continue, with a somewhat larger
429 demographic impact that is negative across all ensemble members. The overall effect
430 on emissions, however, is small and of uncertain sign (ensemble range including both
431 positive and negative changes). This is because the climate impact and even more
432 both CO₂ effects, acting in opposite directions, increase several fold compared to the
433 situation during the 20th century.

434 ***3.2 Driving factors of regional emission changes***

435 By the beginning of the 20th century, the main wildfire emitting region is clearly
436 Africa (Fig. 4), followed by South America, North Asia and Oceania. Emission
437 changes towards the end of the 20th century are mainly due to changes in population
438 density in all regions except for Europe, North America and Oceania where
439 population growth rates are significantly lower. For Europe, climate change has led to
440 an increase in burned area, but an about analogous decrease in fuel load, such that the
441 overall climate effect is small and uncertain. The result for North America is similar,
442 while there is a larger but still uncertain positive CO₂ effect on fuel load, similar to
443 Oceania and South America. For Oceania the population effect is by far the smallest
444 and the only one uncertain in sign (judging by the ensemble range).

445 The climate effect via fuel load is negative in all regions, while the climate effect via
446 burned area is almost always positive, except for the Middle East where it is negative
447 but with a large ensemble range spanning both positive and negative, and South Asia,
448 where it is close to zero. We find a negative CO₂ effect via burned area in the tropics
449 (Africa, South America), but a positive effect in the arid sub-tropics and temperate
450 zones (Middle East, North Asia). The positive climate effect can be explained by
451 regional changes in N_{max} (Table 3, cf. Eq. 1), which are always positive, small for
452 changes during the 20th century, but reaching up to over 100% for Europe from the
453 period 1971-2000 to 2071-2100 under the RCP8.5 climate change scenario. The
454 highest increases are for the northern regions, and the smallest for regions with large
455 deserts, like Africa and Middle East, but starting from a high base. However, climate
456 change can also affect burned area indirectly through vegetation change by changing
457 B or F in Eq. (1), for which a good indicator is the fraction of the total leaf area index
458 that is attributed to grasses ("grass fraction", Table 3). This is because $a(B)$ for
459 grassland and savannahs is about one order of magnitude larger than $a(B)$ for woody

460 biomes (Knorr et al. 2014). There is a general increase in the fraction of woody at the
461 expense of grass vegetation across all except the hyper-arid Middle East region. Here,
462 the grass fraction is by far the highest and the climate too dry to support the expansion
463 of shrubs.

464 For 1971-2000, simulated wildfire emissions are markedly lower than for the
465 beginning of the 20th century for Africa, South America, South Asia and Middle East
466 (Fig. 5). Of these regions, only Africa is predicted to continue to decline for the entire
467 ensemble range for both RCPs. The main drivers are population growth and CO₂
468 impact on burned area, partly compensated by increased fuel load. For South
469 America, South Asia and Oceania the pattern is similar, except with a much smaller
470 demographic impact, resulting in an overall change of uncertain direction.

471 All northern regions (North America, Europe and North Asia) are predicted to
472 increase emissions across the entire ensemble. All of these have a slight positive
473 climate impact, but with large uncertainties, where climate change strongly increases
474 burned area compensated largely by a decrease in fuel load. Since precipitation is
475 predicted to increase in these regions (Table 1), the climate effect is mainly due to
476 increasing temperatures and N_{max} (Tables 1, 3). For North America and North Asia
477 there is a clear positive effect of CO₂ on fuel load which appears to be the main
478 reason for tilting the balance towards emission increases. However, population change
479 plays a rather small role, with a large ensemble range for Europe and North Asia
480 making the sign of the impact uncertain given their slower population growth. For
481 North America, the demographic impact is small, but universally slightly negative. An
482 exception is the region Middle East, which has a large positive CO₂ effect via burned
483 area (cf. Fig. 4).

484 Overall, there is a marked shift in emissions towards the extra-tropics: while for 1971-
485 2000, the tropics have 700 TgC/yr emissions vs. 580 for the extra-tropics (ensemble
486 mean), for 2071-2100 the split ranges between 420 tropics vs. 680 extra-tropics for
487 RCP4.5, high population growth / slow urbanisation, and 600 tropics vs. 720 extra-
488 tropics for RCP8.5, low population growth / fast urbanisation. As the regional
489 analysis shows, this change is mainly the result of expanding population in Africa.
490 However, there is also a much stronger negative climate effect on fuel load at high
491 compared to low latitudes (Fig. 6), which to some degree slows down the shift of
492 emissions to the north. This contrasts with a generally positive CO₂ effect across most
493 of the globe, but with about the same magnitude for tropical and extra-tropical
494 vegetated areas. At high latitudes, combustible fuel load is generally much higher than
495 at low latitudes, implying that this is compensated for by a much smaller burned area,
496 leading to overall lower emissions in this region.

497 ***3.3 Probabilistic forecast of future emission changes***

498 For simulated emissions during the 20th century, we find that a majority of ensemble
499 members show significant increases (i.e. by more than two standard deviations) for
500 northern boreal regions and the Tibetan plateau, and decreases for some scattered
501 regions in Europe and China, but in general, changes are small compared to
502 interannual variability (Fig. 7a). For the 21st century, most simulations for both
503 RCP4.5 (Fig. 7b) and RCP8.5 (Fig. 7c) predict a significant decrease in emissions in
504 Africa, mainly north of the equator, and to a lesser degree and mostly for RCP8.5 for
505 North Australian savannahs. The main regions for which a significant increase in fire
506 emissions is predicted are the boreal-forest / tundra transition zones, Europe and
507 China, and arid regions in Central Australia, southern Africa and Central Asia. For the

508 arid regions, however, the increase is much more pronounced for RCP8.5 than for
509 RCP4.5.

510 These changes in fire emissions during the 21st century relative to current variability
511 can also be analysed by driving factor (Eqs. 4 and 5). The analysis reveals that
512 increases in emissions in the boreal/tundra transitional zone are mostly due to climate
513 change, except for the more continental and arid north-eastern Siberia. For the rest of
514 the globe, the climate effect has a surprisingly small impact, being confined to narrow
515 bands of arid regions in southern Africa, Australia and the Arabian Peninsula. Climate
516 change also leads to a significant decrease in emissions in northern Africa and the
517 Middle East (Fig. 8a-b, cf. Fig. 5). For RCP4.5, CO₂ has only a small positive impact
518 on emissions, mainly for Central Asia, and a negative impact for African, South
519 American and North Australian tropical savannahs. For RCP8.5, the CO₂ effect has a
520 much bigger impact globally on the relative change of emissions, leading to increased
521 emissions in large regions including Mexico, southern South America, all African,
522 Arabian and Central Asian semi-deserts, most of the southern half of Australia, and
523 north-eastern Siberia. The negative effect is also much more pronounced and
524 comprises most tropical savannahs (Fig. 8c-d). This creates opposing effects for the
525 large zone covering North Africa, Arabia and Central Asia, with climate change
526 leading to a decrease in plant productivity and fuel load (hence lower emissions)
527 against CO₂ change leading to CO₂ fertilisation (hence higher emissions).

528 For the moister and in general much more highly emitting savannahs (van der Werf et
529 al. 2010), the dominant effect comes from CO₂ change and is negative, due to shrub
530 encroachment. This creates an interesting situation for Australia: in the very north,
531 higher CO₂ leads to shrub encroachment, leading to lower emissions (Fig. 7); in a
532 central zone across the continent, climate change is the leading driver of increased

533 emissions, but for most of the southern half, CO₂ change leads to enhanced water-use
534 efficiency of the already woody vegetation (Morgan et al. 2007) causing the opposite
535 effect compared to the north. The same pattern is repeated for southern Africa, but
536 with a stronger positive climate effect in the central zone. The demographic effect
537 (Fig. 8e) leads to a significant increase in wildfire emissions in Central and Eastern
538 Europe as well as East Asia due to its projected declining population, but a decrease
539 mainly in African savannahs but also Turkey and Afghanistan/southern Central Asia
540 given their projected large increases in population.

541 **4 Discussion**

542 In this study, we find that wildfire emissions declined likely more than 10% during
543 the course of the 20th century, in agreement with ice core measurements of the
544 isotopic signature of carbon monoxide (Wang et al. 2010). A decline in global
545 wildfire activity since the late 19th century was also suggested by Marlon et al. (2008)
546 based on charcoal records, even though issues remain concerning the magnitude of
547 the decline as and whether there have also been period of increasing emissions (van
548 der Werf et al., 2013). In the present simulations, the decline is caused
549 overwhelmingly by increasing population density, in agreement with the results of
550 Knorr et al. (2014) who used SIMFIRE alone to simulate burned area, without
551 coupling to LPJ-GUESS, driven by the same historical population data. According to
552 the present study, population effects dominated because a positive effect of climate
553 change on burned area was compensated by a negative effect on fuel load, and a
554 negative effect of CO₂ increase on burned area was compensated a positive effect on
555 fuel load. This broad general pattern, found for the main active wildfire regions, is
556 predicted to continue throughout the 21st century, albeit with much stronger climate

557 and CO₂ effects, while the negative population effect on emissions continues to have
558 about the same magnitude.

559 This dominant pattern of opposing climate and CO₂ effects, and opposing effects via
560 burned area and fuel load, calls for a mechanistic explanation. A positive impact of
561 climate change on burned area or numbers of fires is what is commonly expected
562 (Krawchuck et al. 2009, Pechony and Shindell 2010) and it was found for all regions
563 in agreement with simulated changes in fire risk (N_{max} in Eq. 1). The exception is the
564 Middle East region during the 20th century, with a negative climate impact on burned
565 area, which is likely caused by a decline in fuel continuity which suppresses the
566 spread of fires (reduced F in Eq. 1). A negative climate impact on fuel load is
567 consistent with the widely expected positive climate-carbon cycle feedback
568 (Friedlingstein et al. 2006), whereby rising temperatures increase soil and litter
569 respiration rates, releasing CO₂ from the terrestrial biosphere. The faster
570 decomposition of litter under warmer conditions, incorporated into LPJ-GUESS
571 (Smith et al. 2001), leads to a reduction in fuel available for combustion (Knorr et al.
572 2012). Since combustion by fire is nothing more than a shortcut for litter
573 decomposition, higher temperatures simply shift the balance between the two
574 processes towards microbial decomposition. However, the opposite climate effect
575 could also be expected, where warming leads to increased productivity in boreal,
576 temperature-limited ecosystems, leading to increased fuel production (Pausas and
577 Ribeiro 2013). For the present study, at least, this situation does not play a global role
578 and is only found for scattered regions of north-eastern Canada and northern Russia
579 (Fig. 6b).

580 A positive effect of CO₂ on fuel load, which is found to be active almost everywhere
581 across the globe, is fully consistent with the notion of CO₂ fertilisation of the

582 terrestrial biosphere (Long et al. 1996, Körner 2000), whereby higher atmospheric
583 CO₂ concentrations increase the rate of carboxylation, increasing net primary
584 production and thus fuel load (Hickler et al. 2008). However, we also find a negative
585 impact of rising CO₂ on wildfire emissions for all tropical savannah ecosystems,
586 which outweighs the positive impact through increasing fuel load and is caused by an
587 increase in the dominance of woody at the expense of grass vegetation. This
588 phenomenon of shrub encroachment, or woody thickening, in tropical savannahs has
589 been repeatedly observed in field studies (Wigley et al. 2010; Bond and Midgley
590 2012) and frequently attributed to CO₂ enrichment of the atmosphere (Morgan et al.
591 2007; Buitenwerf et al. 2012). This link is less observed for arid savannahs (Bond and
592 Midgley 2012), consistent with the finding here that in the most arid regions, no
593 decrease in the grass fraction is predicted. This result differs partly from that by
594 Lasslop and Kloster (2015), who also found emissions per area burned during the 20th
595 century, but a 40% overall increase in emissions with approximately half of the
596 increase due to increasing burned area.

597 On a global scale, according to the present simulations, the level of future wildfire
598 emissions is highly uncertain for a scenario of moderate greenhouse gas increases
599 (RCP4.5), with the ensemble mean showing slightly lower emissions towards the end
600 of the 21st as opposed to the end of the 20th century. For a high, business-as-usual
601 scenario of greenhouse gas forcing (RCP8.5), the ensemble mean points towards an
602 increase across the same time span, but with a range including both positive and
603 negative changes. There is also a general trend towards increases during the second
604 half of this century. The slight bias towards increased emissions is the result of a
605 combination of increased fire risk due to warming, and increased fuel load due to CO₂
606 fertilisation, but with population growth, woody thickening and faster litter

607 decomposition all counteracting. We therefore find that climatic impacts on fire risk
608 are only one of many, often opposing factors that might lead to increased wildfire
609 emissions in the future.

610 The future demographic dynamics can lead to a wide range of future wildfire
611 emissions. In addition to its indirect impact on wildfire emissions through interactions
612 with economic and technological changes contributing to GHGs emissions and
613 climate change, changes in population size and spatial distribution play a direct and
614 important role for fire prevalence, as an ignition source but predominantly as fire
615 suppressors. While fertility decline is occurring in almost all global regions, the
616 population momentum will continue to drive global population size upward for at
617 least some years and likely contribute to continuously declining wildfire frequencies.

618 The uncertainty of future population dynamics, however, leads to a wide range of
619 population trends and causes large variations in simulated wildfire emissions.

620 Moreover, the same changes in population sizes can result in rather different
621 emissions due to variations in spatial population distribution, particularly through
622 different urbanisation patterns. While the whole world is expected to be further
623 urbanised, variations in speed and patterns of urbanisation across regions and over
624 time can lead to significantly different wildfire patterns.

625 Simulated emissions presented here generally agree with similar results with a
626 coupled fire-vegetation-biogeochemical model by Kloster et al. (2012), insofar as
627 climate only starts to impact on fire during the course of the 21st century, but not
628 before, and that changes in population density generally lead to lower emissions. The
629 difference is that in the present study, climate has a much smaller impact on
630 emissions, ranging between 0 and +20% for RCP8.5 and few percent at most for
631 RCP4.5. A similar study reporting simulations of increasing fire emissions for Europe

632 (Migliavacca et al. 2013a) reports an increase for Europe of about 15 TgC yr⁻¹ until
633 the late 21st century, when measured for the same reference period as here, which is
634 within the ensemble range found in this study. Even though they used the same
635 Community Land Model, their fire parameterisation (Migliavacca et al. 2013b)
636 differed from the one used by Kloster et al. (2012).

637 The difference between the present study and the one by Kloster and co-workers
638 might be due to the pronounced negative effect of temperature change on fuel load,
639 and of CO₂ on burned area, found here. Another important difference is their study
640 included deforestation fires, and employed the more common approach of
641 representing the impact of population density by a combination of number of ignitions
642 times an explicit function of fire suppression, the combination of which leads to a
643 small decrease in emissions during the 21st century. This approach, based on
644 Venevsky et al. (2002), always leads to an increase in burned area if ignitions increase,
645 all else being equal. No decline is simulated during the 20th century, neither due to
646 changing population density, nor land use. This study, by contrast, uses a semi-
647 empirical approach with a functional form of the relationship between burned area
648 and population density derived by optimisation against observed burned area and
649 simulates the historical decline that is suggested on the basis of ice core and charcoal
650 records. The implicit assumption here is that that for most of the world, except for
651 areas where population density is very low, the fire regime is ignition saturated
652 (Guyette et al. 2002), in contradiction to the approach by Venevsky et al. (2002).

653 This means that above a threshold of typically 0.1 inhabitants per km², burned area
654 becomes independent of human population density (cf. Knorr et al. 2014). However,
655 if we assume some increase in burned area with population density below the
656 threshold, the results change only little (Fig. 3). Therefore we argue for universal

657 ignition saturation as a reasonable approximation at the scales considered in the
658 present study. We also expect possible future increases in lightning activity (Romps et
659 al. 2014) to have only a marginal effect on burned area and thus emissions.

660 An important outcome of this study is that it predicts are large shift in fire emissions
661 from the tropics towards the extra-tropics, driven by two coinciding effects causing a
662 secular decline in emissions in African savannahs and grasslands: CO₂ increases
663 driving woody thickening, in turn making the vegetation less flammable (Bond and
664 Midgley 2012), and population growth leading to decreased burned area (Archibald et
665 al. 2008). The impact of this shift on the global budget of carbon emissions from
666 wildfires is so large because these regions currently have by far the largest emissions
667 worldwide (van der Werf et al. 2010). In agreement with observed evidence (Bond
668 and Midgley 2012), the negative CO₂ effect on emissions via burned area is limited to
669 the semi-humid tropics and does not play a role either in the most arid regions, nor at
670 higher latitudes. It is also not simulated for South Asia, where most of the potential
671 semi-humid grasslands and savannahs have long been converted to agriculture. For
672 the mostly arid region Middle East, we find that a strong positive CO₂ effect via
673 burned area is the larger contributor to emission change during the 20th century, and
674 the biggest during the 21st. This leads to a marked increase in emissions for RCP8.5,
675 outcompeting negative impacts of growing population and climate change on fuel
676 load and driven by a marked decline in precipitation (Table 1), while during the 20th
677 century, there is a marked negative impact of climate change on burned area. Here,
678 CO₂ fertilisation leads to denser vegetation, increasing fuel continuity (higher F in Eq.
679 1), thus leading to higher burned area, while decreasing precipitation results in a
680 lower F . To a lesser extent this is simulated for North Asia, which also contains large,
681 highly arid regions, but with a positive ensemble-mean climate effect on burned area.

682 For both regions, however, the ensemble spread is very large making the projections
683 highly uncertain.

684 For Australia, we find an interesting zonal pattern of changing effects from the
685 northern savannahs to the arid southern coast. In the very north, woody thickening
686 due to higher CO₂ leads to decreased emissions through decreased burned area, with
687 negligible climate effects. This is followed by a central zone where both climate and
688 CO₂ change lead to increased emissions, and a third zone comprising the southern half
689 of the Australian interior where CO₂ fertilisation leads to increased emissions via
690 higher productivity. Population change plays almost no role for changing emissions in
691 this region. As a result, the north is predicted to decrease significantly in emissions,
692 while for the central zone where climate and CO₂ effects overlap, and for the south
693 there is no clear signal in the prediction. A similar tri-zonal pattern is also predicted
694 for southern Africa stretching from the Miombo woodlands across the Kalahari to the
695 Cape region. This zonal differentiation resembles the results by Kelley and Harrison
696 (2014), who simulated a reduction in burned area in North Australia due to CO₂
697 driven woody thickening, but an increase in burned area in the Australian interior due
698 to enhanced fuel continuity with denser vegetation caused by CO₂ fertilisation.

699 **5 Conclusions**

700 We find that since the early 20th century, wildfire emissions have been steadily
701 declining due to expanding human population, but that this decline will only continue
702 if climate change and atmospheric CO₂ rise is limited to low or low/moderate levels,
703 population continues to grow and urbanisation follows a slow pathway in the next
704 decades. Otherwise, it is likely that the world is currently in a historic minimum
705 regarding wildfire emissions, and the current declining emission trend will reverse in
706 the future at higher latitudes, departing from the current domination of African

707 savannahs. Emissions, however, are unlikely until 2100 to again reach early 20th
708 century levels. The predictions are based on an ensemble of climate and
709 population/urbanisation projections, but a single fire model albeit tested for the impact
710 of different parameterisations. The results generally show a large ensemble spread,
711 and also reveal widely opposing factors influencing future emissions, complicating
712 the task of predicting future wildfire emissions. We find that apart from climate
713 leading to higher fire risk, equally important factors on a global scale are demographic
714 change, woody thickening in savannahs with higher CO₂ levels, and faster woody or
715 grass litter turnover in a warmer climate, both leading to declining emission, as well
716 as CO₂ fertilisation generally leading to higher fuel loads or fuel continuity and thus
717 increased emissions. Therefore, the common view of climate warming as the
718 dominant driver of higher future wildfire emissions cannot be supported.

719 This work is assumes that fire management for a given fire and vegetation regime
720 will remain unchanged. New fire policies that go beyond simple fire suppression
721 and thus avoid large-scale fuel build-up and ultimately increased risks of large
722 fires could very well counteract the effects of climate change and thus lead to
723 a better co-existence between humans, natural ecosystems and wildfires.

724 **Author contribution**

725 W. K. conceived the study, carried out model runs, performed the analysis and wrote
726 the first full draft of the manuscript, L. J. provided the population scenarios, all
727 authors contributed to discussions of results and writing.

728 **Acknowledgements**

729 This work was supported by EU contracts 265148 (Pan-European Gas-Aerosol-
730 climate interaction Study, PEGASOS) and grant 603542 (Land-use change: assessing
731 the net climate forcing, and options for climate change mitigation and adaptation,
732 LUC4C). We thank Thomas Hickler for pointing out relevant literature on woody
733 thickening.

734 **References**

- 735 Ahlström, A., Schurgers, G., Arneth, A., and Smith, B.: Robustness and uncertainty in
736 terrestrial ecosystem carbon response to CMIP5 climate change projections, *Env.*
737 *Res. Lett.*, 7, 044008, doi:10.1088/1748-9326/7/4/044008, 2012.
- 738 Andela, N. and van der Werf, G. R.: Recent trends in African fires driven by cropland
739 expansion and El Nino to La Nina transition, *Nature Climate Change*, 4, 791-795,
740 2014.
- 741 Archibald, S., Roy, D. P., van Wilgen, B. W., and Scholes, R. J.: What limits fire? An
742 examination of drivers of burnt area in Southern Africa, *Global Change Biol*, 15,
743 613-630, 2008.
- 744 Arneth, A., Harrison, S. P., Zaehle, S., Tsigaridis, K., Menon, S., Bartlein, P. J.,
745 Feichter, J., Korhola, A., Kulmala, M., O'Donnell, D., Schurgers, G., Sorvari, S.,
746 and Vesala, T.: Terrestrial biogeochemical feedbacks in the climate system, *Nat*
747 *Geosci*, 3, 525-532, 2010.
- 748 Bistinas, I., Harrison, D. E., Prentice, I. C., and Pereira, J. M. C.: Causal relationships
749 vs. emergent patterns in the global controls of fire frequency, *Biogeosci.*, 11,
750 5087–5101, doi:10.5194/bg-11-5087-2014, 2014.
- 751 Bond, W. J. and Midgley, G. F.: Carbon dioxide and the uneasy interactions of trees
752 and savannah grasses, *Phil. Trans. R. Soc. B*, 367, 601-612, 2012.

753 Bowman, D. M. J. S., Balch, J. K., Artaxo, P., Bond, W. J., Carlson, J. M., Cochrane,
754 M. A., D'Antonio, C. M., DeFries, R. S., Doyle, J. C., Harrison, S. P., Johnston, F.
755 H., Keeley, J. E., Krawchuk, M. A., Kull, C. A., Marston, J. B., Moritz, M. A.,
756 Prentice, I. C., Roos, C. I., Scott, A. C., Swetnam, T. W., van der Werf, G. R., and
757 Pyne, S. J.: Fire in the Earth System, *Science*, 324, 481-484, 2009.

758 Buitenwerf, R., Bond, W. J., Stevens, N., and Trollope, W. S. W.: Increased tree
759 densities in South African savannas: > 50 years of data suggests CO₂ as a driver,
760 *Global Change Biol*, 18, 675-684, 2012.

761 Claussen, M., Brovkin, V., and Ganopolski, A.: Biogeophysical versus
762 biogeochemical feedbacks of large-scale land cover change, *Geophys. Res. Let.*,
763 28, 1011-1014, 2001.

764 Friedlingstein, P., Cox, P. M., Betts, R. A., Bopp, L., von Bloh, W., Brovkin, V.,
765 Cadule, P., Doney, S., Eby, M., Fung, I., Bala, G., John, J., Jones, C. D., Joos, F.,
766 Kato, T., Kawamiya, M., Knorr, W., Lindsay, K., Matthews, H. D., Raddatz, T.,
767 Rayner, P. J., Reick, C., Roeckner, E., Schnitzler, K.-G., Schnur, R., Strassmann,
768 K., Weaver, A. J., Yoshikawa, C., and Zeng, N.: Climate-carbon cycle feedback
769 analysis, results from the C4MIP model intercomparison, *J. Climate*, 19, 3337-
770 3353, 2006.

771 Giglio, L., Randerson, J. T., van der Werf, G. R., Kasibhatla, P. S., Collatz, G. J.,
772 Morton, D. C., and DeFries, R. S.: Assessing variability and long-term trends in
773 burned area by merging multiple satellite fire products *Biogeosci.*, 7, 1171-1186,
774 2010.

775 Giglio, L., Randerson, J. T., and van der Werf, G. R.: Analysis of daily, monthly, and
776 annual burned area using the fourth-generation global fire emissions database
777 (GFED4), *J Geophys Res-Bioge*, 118, 317-328, 2013.

778 Guyette, R. P., Muzika, R. M., and Dey, D. C.: Dynamics of an anthropogenic fire
779 regime, *Ecosystems*, 5, 472-486, 2002.

780 Harris, I., Jones, P. D., Osborn, T. J., and Lister, D. H.: Updated high-resolution grids
781 of monthly climatic observations – the CRU TS3.10 Dataset, *Int. J. Climatol.*, 34,
782 623-642, 2014.

783 Hickler, T., Smith, B., Prentice, I. C., Mjöfors, K., Miller, P., Arneth, A., and Sykes,
784 M. T.: CO₂ fertilization in temperate FACE experiments not representative of
785 boreal and tropical forests, *Global Change Biol*, 14, 1531-1542, 2008.

786 Hurtt, G. C., Chini, L. P., Frohking, S., Betts, R. A., Feddema, J., Fischer, G., Fisk, J.
787 P., Hibbard, K., Houghton, R. A., Janetos, A., Jones, C. D., Kindermann, G.,
788 Kinoshita, T., Goldewijk, K. K., Riahi, K., Shevliakova, E., Smith, S., Stehfest, E.,
789 Thomson, A., Thornton, P., van Vuuren, D. P., and Wang, Y. P.: Harmonization of
790 land-use scenarios for the period 1500-2100: 600 years of global gridded annual
791 land-use transitions, wood harvest, and resulting secondary lands, *Climatic
792 Change*, 109, 117-161, 2011.

793 Jiang, L.: Internal consistency of demographic assumptions in the shared
794 socioeconomic pathways, *Popul. Environ.*, 35, 261-285, 2014.

795 Kasischke, E. S. and Penner, J. E.: Improving global estimates of atmospheric
796 emissions from biomass burning, *J. Geophys. Res.*, 109, D14S01,
797 doi:10.1029/2004JD004972, 2004.

798 Klein Goldewijk, K., Beusen, A., and Janssen, P.: Long-term dynamic modeling of
799 global population and built-up area in a spatially explicit way: HYDE 3.1,
800 *Holocene*, 20, 565-573, 2010.

801 Kloster, S., Mahowald, N. M., Randerson, J. T., and Lawrence, P. J.: The impacts of
802 climate, land use, and demography on fires during the 21st century simulated by
803 CLM-CN, *Biogeosciences*, 9, 509-525, 2012.

804 Knorr, W., Lehsten, V., and Arneth, A.: Determinants and predictability of global
805 wildfire emissions, *Atm. Chem. Phys.*, 12, 6845–6861, 2012.

806 Knorr, W., Kaminski, T., Arneth, A., and Weber, U.: Impact of human population
807 density on fire frequency at the global scale, *Biogeosci.*, 11, 1085-1102, 2014.

808 Knorr, W., Jiang, L., Arneth, A. Demographic controls of future fire risk, *submitted*.

809 Körner, C.: Biosphere responses to CO₂ enrichment, *Ecological Applications*, 10,
810 1590-1619, 2000.

811 Krawchuk, M. A., Moritz, M. A., Parisien, M. A., Van Dorn, J., and Hayhoe, K.:
812 Global Pyrogeography: the Current and Future Distribution of Wildfire, *Plos One*,
813 4, e5102, doi:10.1371/journal.pone.0005102, 2009.

814 Langmann, B., Duncan, B., Textor, C., Trentmann, J., and van der Werf, G. R.:
815 Vegetation fire emissions and their impact on air pollution and climate, *Atmos*
816 *Environ*, 43, 107-116, 2009.

817 Long, S. P., Osborne, C. P., and Humphries, S. W.: Photosynthesis, rising
818 atmospheric carbon dioxide concentration and climate change. In: *Global change:*
819 *Effects on coniferous forests and grasslands*, Breymeyer, A. I., Hall, D. O.,
820 Melillo, J. M., and Ågren, G. I. (Eds.), Scope, Wiley & Sons, New York, 1996.

821 Marlon, J. R., Bartlein, P. J., Carcaillet, C., Gavin, D. G., Harrison, S. P., Higuera, P.
822 E., Joos, F., Power, M. J., and Prentice, I. C.: Climate and human influences on
823 global biomass burning over the past two millennia, *Nature Geosci.*, 1, 697-702,
824 2008.

825 Martin Calvo, M. and Prentice, I. C.: Effects of fire and CO₂ on biogeography and
826 primary production in glacial and modern climates, *New Phytologist*, 208, 987-
827 994, 2015.

828 Meinshausen, M., Smith, S. J., Calvin, K., Daniel, J. S., Kainuma, M. L. T.,
829 Lamarque, J.-F., Matsumoto, K., Montzka, S. A., Raper, S. C. B., Riahi, K.,
830 Thomson, A., Velders, G. J. M., and van Vuuren, D. P. P.: The RCP greenhouse
831 gas concentrations and their extensions from 1765 to 2300, *Climatic Change*, 109,
832 213-241, 2011.

833 Migliavacca, M., Dosio, A., Camia, A., Hobourg, R., Houston Durtant, T., Kaiser, J.
834 W., Khabarov, N., Krasovskii, A. A., Marcolla, B., Miguel-Ayanz, J., Ward, D. S.,
835 and Cescatti, A.: Modeling biomass burning and related carbon emissions during
836 the 21st century in Europe, *J. Geophys. Res.*, 118, 1732–1747, 2013a.

837 Migliavacca, M., Dosio, A., Kloster, S., Ward, D. S., Camia, A., Houborg, R.,
838 Houston Durtant, T., Khabarov, N., Krasovskii, A. A., San Miguel-Ayanz, J., and
839 Cescatti, A.: Modeling burned area in Europe with the Community Land Model, *J*
840 *Geophys Res*, 118, 265–279, 2013b.

841 Morgan, J. A., Milchunas, D. G., LeCain, D. R., West, M., and Mosier, A. R.: Carbon
842 dioxide enrichment alters plant community structure and accelerates shrub growth
843 in the shortgrass steppe, *Proc. Nat. Acad. Sci. USA*, 104, 14724-14729, 2007.

844 Moritz, M. A., Parisien, M.-A., Batllori, E., Krawchuk, M. A., Van Dorn, J., Ganz, D.
845 J., and Hayhoe, K.: Climate change and disruptions to global fire activity,
846 *Ecosphere*, 3, 49, doi:10.1890/ES11-00345.1, 2012.

847 O'Neill, B., Carter, T. R., Ebi, K. L., Edmonds, J., Hallegatte, S., Kemp-Benedict, E.,
848 Kriegler, E., Mearns, L., Moss, R., Riahi, K., van Ruijven, B., and van Vuuren, D.:
849 Workshop on The Nature and Use of New Socioeconomic Pathways for Climate

850 Change Research, Boulder, CO, November 2–4 2011, available at:
851 [https://www2.cgd.ucar.edu/sites/default/files/iconics/Boulder-Workshop-](https://www2.cgd.ucar.edu/sites/default/files/iconics/Boulder-Workshop-Report.pdf)
852 [Report.pdf](https://www2.cgd.ucar.edu/sites/default/files/iconics/Boulder-Workshop-Report.pdf) (last access: 9 September 2015, National Center for Atmospheric
853 Research (NCAR), Boulder, CO, 2012.

854 Pechony, O. and Shindell, D. T.: Driving forces of global wildfires over the past
855 millennium and the forthcoming century, *Proc. Natl. Acad. Sci. USA*, 107, 19167-
856 19170, 2010.

857 Pausas, J. G. and Ribeiro, E.: The global fire–productivity relationship, *Global Ecol*
858 *Biogeogr*, 22, 728-736, 2013.

859 Ramankutty, N. and Foley, J. A.: Estimating historical changes in global land cover:
860 Croplands from 1700 to 1992, *Global Biogeochemical Cycles*, 13, 997-1027, 1999.

861 Randerson, J., Chen, Y., van der Werf, G. R., Rogers, B. M., and Morton, D. C.:
862 Global burned area and biomass burning emissions from small fires, *J. Geophys.*
863 *Res.*, 117, G04012, doi:10.1029/2012JG002128, 2012.

864 Romps, D. M., Seeley, J. T., Vollaro, D., and Molinari, J.: Projected increase in
865 lightning strikes in the United States due to global warming, *Science*, 346, 851-
866 854, 2014.

867 Roy, D. P., Boschetti, L., Justice, C. O., and Ju, J.: The collection 5 MODIS burned
868 area product - Global evaluation by comparison with the MODIS active fire
869 product, *Remote Sens Environ*, 112, 3690-3707, 2008.

870 Scholze, M., Knorr, W., Arnell, N. W., and Prentice, I. C.: A climate-change risk
871 analysis for world ecosystems, *Proc. Nat. Acad. Sci. USA*, 103, 13116-13120,
872 2006.

873 Smith, B., Prentice, C., and Sykes, M.: Representation of vegetation dynamics in
874 modelling of terrestrial ecosystems: comparing two contrasting approaches within

875 European climate space, *Global Ecol Biogeogr*, 10, 621-637, 2001.

876 Stein, U. and Alpert, P.: Factor separation in numerical simulations, *Journal of the*
877 *Atmospheric Sciences*, 50, 2107-2115, 1993.

878 Taylor, K. E., Stouffer, R. J., and Meehl, G. A.: An overview of CMIP5 and the
879 experiment design, *Bull. Am. Meteorol. Soc.*, 93, 485-498, 2012.

880 Thonicke, K., Spessa, A., Prentice, I. C., Harrison, S. P., Dong, L., and Carmona-
881 Moreno, C.: The influence of vegetation, fire spread and fire behaviour on biomass
882 burning and trace gas emissions: results from a process-based model,
883 *Biogeosciences*, 7, 1991-2011, 2010.

884 van der Werf, G. R., Randerson, J. T., Giglio, L., Collatz, G. J., Mu, M., Kasibhatla,
885 P. S., Morton, D. C., Defries, R. S., Jin, Y., and van Leeuwen, T. T.: Global fire
886 emissions and the contribution of deforestation, savanna, forest, agricultural, and
887 peat fires (1997-2009), *Atmos. Chem. Phys.*, 10, 11707-11735, 2010.

888 van der Werf, G. R., Peters, W., van Leeuwen, T. T., and Giglio, L.: What could have
889 caused pre-industrial biomass burning emissions to exceed current rates?, *Clim.*
890 *Past*, 9, 289-306, 2013.

891 van Vuuren, A. J., Edmonds, J., Kainuma, M., Riahi, K., Thomson, A., Hibbard, K.,
892 Hurtt, G. C., Kram, T., Krey, V., Lamarque, J. F., Masui, T., Meinshausen, M.,
893 Naicenovic, N., Smith, S. J., and Rose, S. K.: The representative concentration
894 pathways: an overview, *Clim. Change*, 109, 5-31, 2011.

895 Venevsky, S., Thonicke, K., Sitch, S., and Cramer, W.: Simulating fire regimes in
896 human-dominated ecosystems: Iberian Peninsula case study, *Global Change*
897 *Biology*, 8, 984-998, 2002.

898 Wang, Z., Chappellaz, J., Park, K., and Mak, J. E.: Large variations in Southern
899 Hemisphere biomass burning during the last 650 years, *Science*, 330, 1663-1666,

900 2010.

901 Wigley, B. J., Bond, W. J., and Hoffman, M. T.: Thicket expansion in a South African

902 savanna under divergent land use: local vs. global drivers?, *Global Change Biol.*,

903 16, 964-976, 2010.

904 **Tables**

905 *Table 1: Simulated changes in climate by region*.*

Absolute change in annual-mean temperature [K]*									
Region	historical ⁽¹⁾			RCP4.5 ⁽²⁾			RCP8.5 ⁽²⁾		
North America	0.62	(0.03,	1.18)	3.15	(1.88,	4.90)	5.70	(3.78,	7.97)
Europe	0.50	(-0.20,	1.00)	2.56	(1.77,	3.83)	4.53	(3.46,	6.26)
North Asia	0.51	(0.07,	0.98)	3.25	(2.13,	4.81)	5.69	(3.91,	7.63)
Middle East	0.50	(0.09,	0.86)	2.71	(1.82,	3.78)	5.05	(3.68,	6.33)
South America	0.43	(0.07,	0.78)	2.36	(1.65,	3.19)	4.34	(2.83,	5.39)
Africa	0.47	(0.08,	0.72)	2.54	(1.77,	3.34)	4.67	(3.48,	5.87)
South Asia	0.37	(0.01,	0.65)	2.28	(1.60,	3.06)	4.07	(2.95,	5.09)
Oceania	0.44	(0.17,	0.74)	2.18	(1.35,	2.83)	4.16	(2.83,	5.35)
Globe	0.50	(0.08,	0.83)	2.77	(1.83,	3.89)	5.01	(3.49,	6.48)
Relative change in mean annual precipitation*									
North America	-0.5%	(-1.8%,	1.6%)	4.6%	(-2.1%,	7.6%)	5.3%	(-5.7%,	10.8%)
Europe	-1.0%	(-4.5%,	1.5%)	1.9%	(-3.0%,	10.7%)	0.6%	(-5.6%,	13.1%)
North Asia	-0.8%	(-3.3%,	1.0%)	9.4%	(5.8%,	15.1%)	13.8%	(8.2%,	19.7%)
Middle East	-6.4%	(-11.8%,	0.9%)	-6.0%	(-17.0%,	5.7%)	-10.7%	(-28.3%,	0.0%)
South America	-2.5%	(-6.8%,	-0.9%)	-0.7%	(-8.8%,	11.7%)	-1.3%	(-10.6%,	14.3%)
Africa	-2.7%	(-9.3%,	0.1%)	1.4%	(-6.3%,	5.0%)	2.7%	(-5.0%,	9.6%)
South Asia	-1.2%	(-6.0%,	1.8%)	8.3%	(4.9%,	12.8%)	14.5%	(9.0%,	22.3%)
Oceania	-1.5%	(-7.2%,	2.7%)	-1.9%	(-27.2%,	6.6%)	-6.7%	(-38.3%,	11.8%)
Globe	-1.8%	(-3.2%,	0.1%)	3.3%	(-1.1%,	5.6%)	4.7%	(0.8%,	7.6%)

* Mean across 8-ESM ensemble, ensemble minimum and maximum in parentheses.

⁽¹⁾ Changes from 1901-1930 to 1971-2000.

⁽²⁾ Changes from 1971-2000 to 2071-2100.

906 *Table 2: Temporal average of global wildfire emissions in TgC/yr by time period, scenario and ESM*.*

Period	RCP	Population growth	Urbanization	ESM Ensemble	MPI-ESM-LR ⁽¹⁾	CCSM4 ⁽²⁾	CSIRO-Mk3.6 ⁽³⁾	EC-EARTH ⁽⁴⁾	CNRM-CM5 ⁽⁵⁾	GISS-E2-R ⁽⁶⁾	IPSL-CM5A-MR ⁽⁷⁾	HADGEM2-ES ⁽⁸⁾
1901-1930	-	Historical	Historical	1.43	1.44	1.42	1.46	1.42	1.43	1.42	1.44	1.39
1971-2000				<i>1.28</i>	<i>1.32</i>	<i>1.27</i>	<i>1.28</i>	<i>1.29</i>	<i>1.29</i>	<i>1.25</i>	<i>1.28</i>	<i>1.27</i>
2071-2100	4.5	low	fast	1.31	1.36	1.31	1.27	1.31	1.29	1.27	1.33	1.36
		intermediate	fast	1.27	1.32	1.27	1.23	1.26	1.26	1.23	1.29	1.32
		intermediate	central	1.22	1.26	1.22	1.17	1.20	1.20	1.18	1.23	1.27
		intermediate	slow	1.17	1.21	1.16	1.13	1.15	1.15	1.13	1.18	1.21
		high	slow	1.11	1.15	1.11	1.07	1.09	1.09	1.07	1.12	1.16
	8.5	low	fast	1.43	1.52	1.45	1.41	1.38	1.41	1.37	1.42	1.50
		intermediate	fast	1.39	1.47	1.41	1.38	1.34	1.36	1.33	1.38	1.46
		intermediate	central	1.33	1.41	1.36	1.32	1.29	1.30	1.28	1.33	1.40
		intermediate	slow	1.28	1.35	1.31	1.26	1.24	1.25	1.23	1.27	1.35
		high	slow	1.22	1.29	1.24	1.19	1.18	1.19	1.18	1.22	1.28

¹⁾ Max Planck Institute for Meteorology; ²⁾ National Centre for Atmospheric Research

³⁾ Commonwealth Scientific and Industrial Research Organization in collaboration with Queensland CSIRO Climate Change Centre of Excellence

⁴⁾ EC-EARTH consortium

⁵⁾ Centre National de Recherches Météorologiques / Centre Européen de Recherche et Formation Avancée en Calcul Scientifique

⁶⁾ NASA Goddard Institute for Space Studies; ⁷⁾ Institut Pierre-Simon Laplace; ⁸⁾ Met Office Hadley Centre

* Emissions larger than during 1971-2000 (italics) are shown in bold.

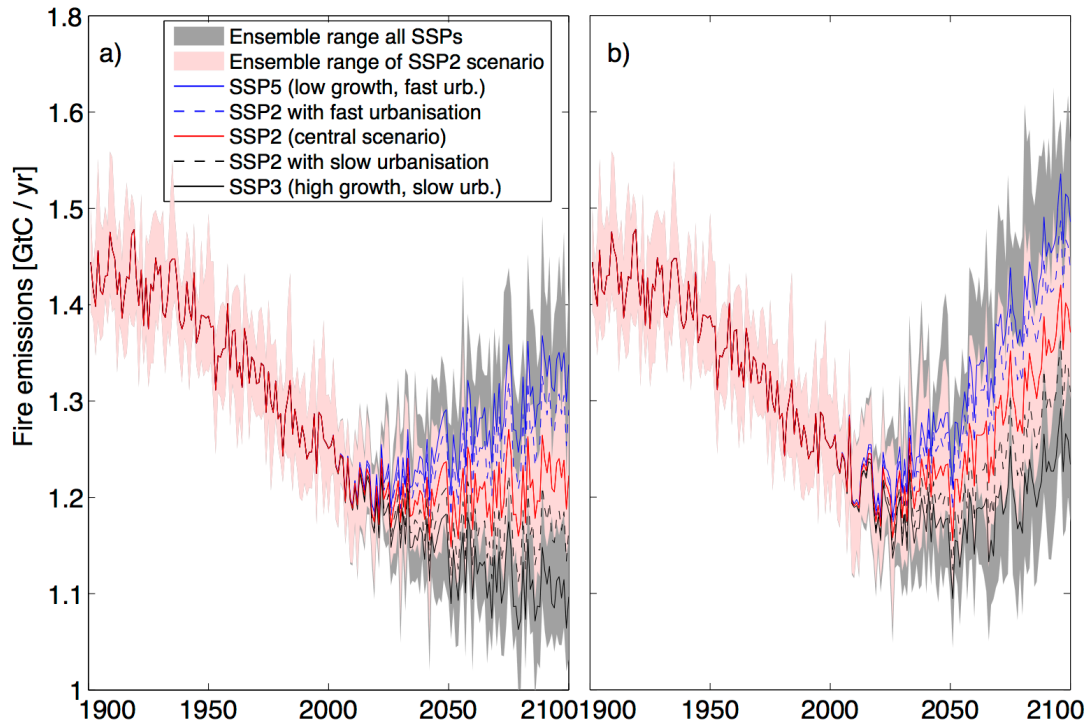
908 Table 3: Changes in climatic and vegetation fire risk*

<i>Mean annual-maximum Nesterov index</i>												
Region	1901-1930			1971-2000			RCP4.5 ⁽¹⁾			RCP8.5 ⁽¹⁾		
North America	153	(143,	165)	160	(148,	170)	204	(178,	236)	250	(211,	327)
Europe	80	(73,	93)	83	(77,	87)	120	(94,	152)	166	(103,	228)
North Asia	146	(142,	154)	149	(144,	155)	188	(163,	220)	227	(185,	292)
Middle East	2878	(2731,	3184)	2923	(2831,	3169)	3201	(2962,	3443)	3401	(3060,	3776)
South America	240	(223,	254)	248	(233,	272)	298	(258,	338)	348	(265,	432)
Africa	1461	(1379,	1491)	1481	(1434,	1530)	1618	(1519,	1728)	1719	(1566,	1898)
South Asia	288	(272,	314)	296	(276,	318)	332	(300,	368)	368	(312,	449)
Oceania	570	(509,	605)	586	(535,	625)	671	(553,	851)	795	(598,	1085)
Globe	726	(700,	765)	740	(715,	773)	827	(767,	878)	903	(817,	1007)
<i>Grass fraction</i>												
North America	30%	(28%,	31%)	28%	(27%,	29%)	22%	(20%,	23%)	20%	(19%,	22%)
Europe	14%	(13%,	15%)	12%	(11%,	13%)	10%	(9%,	12%)	11%	(9%,	12%)
North Asia	36%	(34%,	37%)	33%	(33%,	34%)	21%	(17%,	23%)	16%	(13%,	18%)
Middle East	75%	(74%,	76%)	76%	(75%,	77%)	77%	(76%,	79%)	76%	(75%,	78%)
South America	26%	(25%,	28%)	23%	(23%,	24%)	16%	(15%,	16%)	13%	(12%,	14%)
Africa	57%	(56%,	59%)	53%	(53%,	54%)	40%	(39%,	42%)	34%	(32%,	36%)
South Asia	26%	(25%,	27%)	23%	(23%,	24%)	17%	(16%,	18%)	15%	(14%,	15%)
Oceania	82%	(79%,	85%)	81%	(79%,	83%)	76%	(74%,	81%)	69%	(65%,	76%)
Globe	43%	(43%,	44%)	41%	(41%,	41%)	33%	(32%,	34%)	29%	(28%,	31%)

* Mean across 8-ESM ensemble, ensemble minimum and maximum in parentheses.

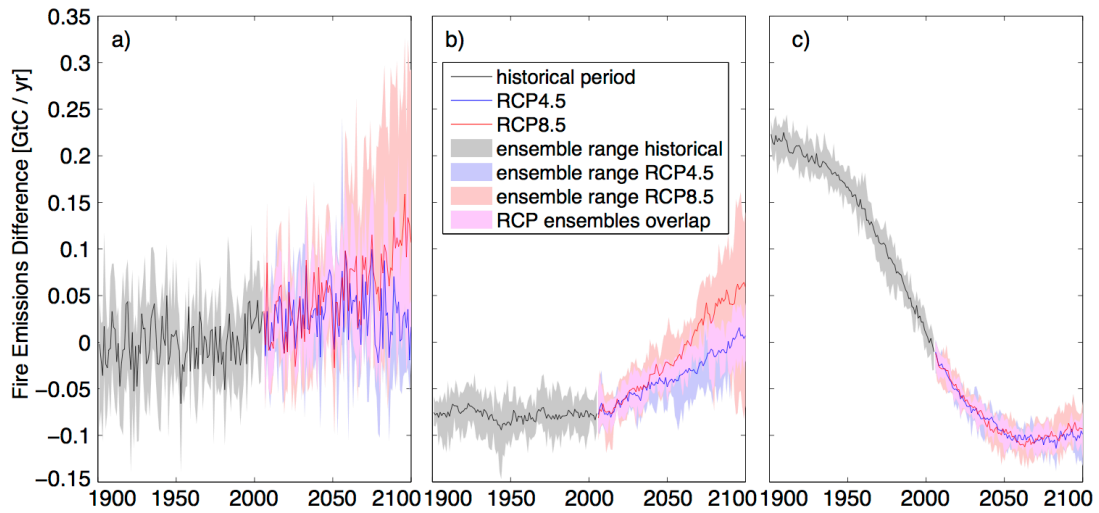
⁽¹⁾ Temporal average for 2071-2100.

909 **Figures**



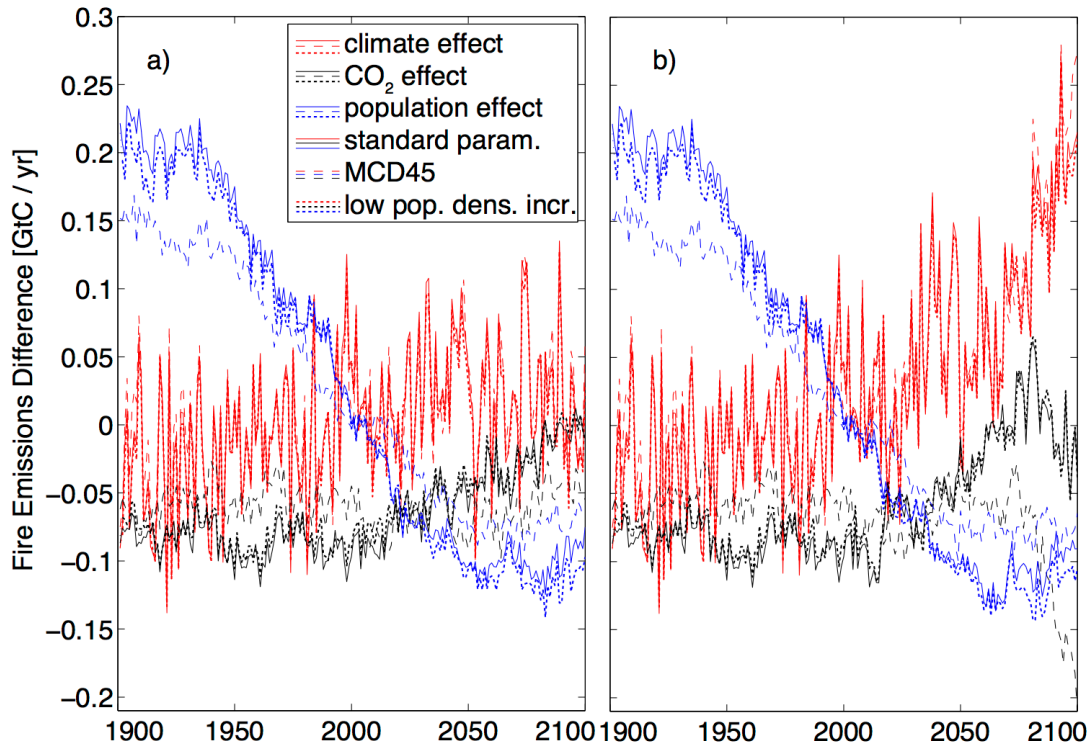
910
911 *Figure 1: Simulated global wildfire emissions 1900 to 2100. Shaded areas are for the*
912 *range of ensemble members either across all ESMs using only the central population*
913 *scenario SSP2, or across ESMs and all population scenarios. Lines show ensemble*
914 *averages for specific population scenarios. a) RCP4.5 greenhouse gas concentrations*
915 *and climate change; b) RCP8.5.*

916



917

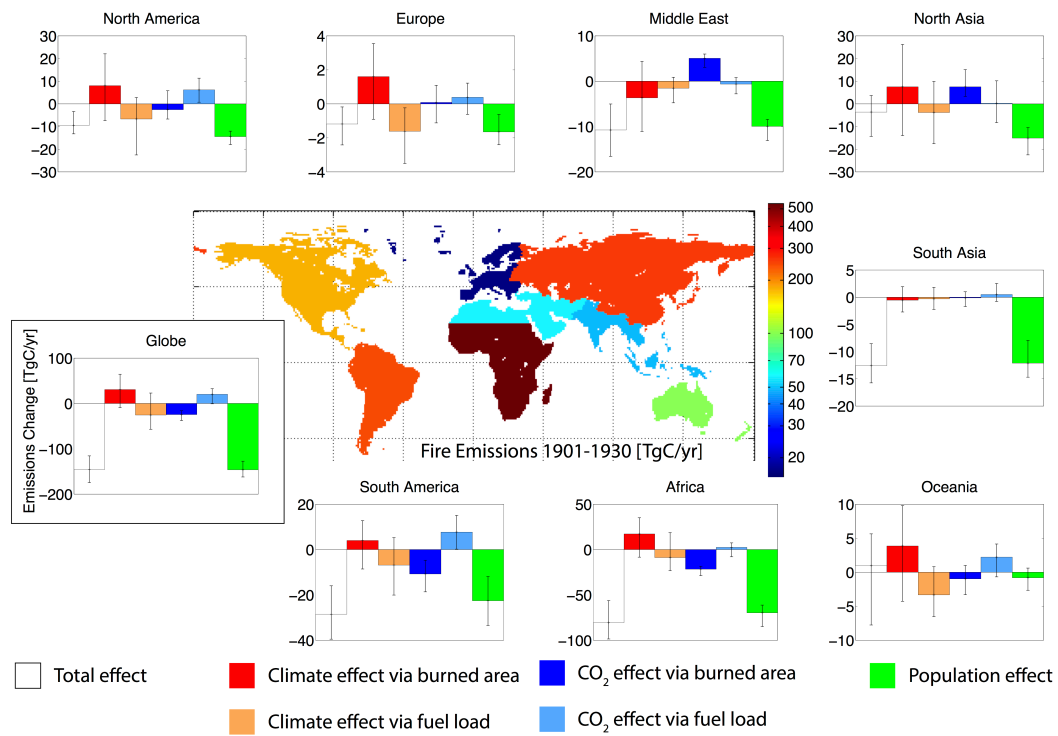
918 *Figure 2: Effects of different factors on global emissions for historical change (until*
 919 *2005) and two future climate change scenarios (RCP4.5 and RCP8.5). a) Effect of*
 920 *climate change, b) effect of changing atmospheric CO₂, c) effect of changing human*
 921 *population density. All simulations are for the central SSP2 population scenario.*
 922 *Solid lines for ESM ensemble means and shaded areas for the range across eight*
 923 *ESM simulations each.*



924

925 *Figure 3: Impact of changing fire model parameterisation on the simulated climate,*
 926 *CO₂ and population effects on emissions. Standard parameterisation of SIMFIRE*
 927 *optimised against GFED3 burned area, optimisation against MCD45 burned area,*
 928 *and simulation assuming an increasing effect of population density on burned area*
 929 *between 0 and 0.1 inhabitants / km². a) RCP4.5. b) RCP8.5.*

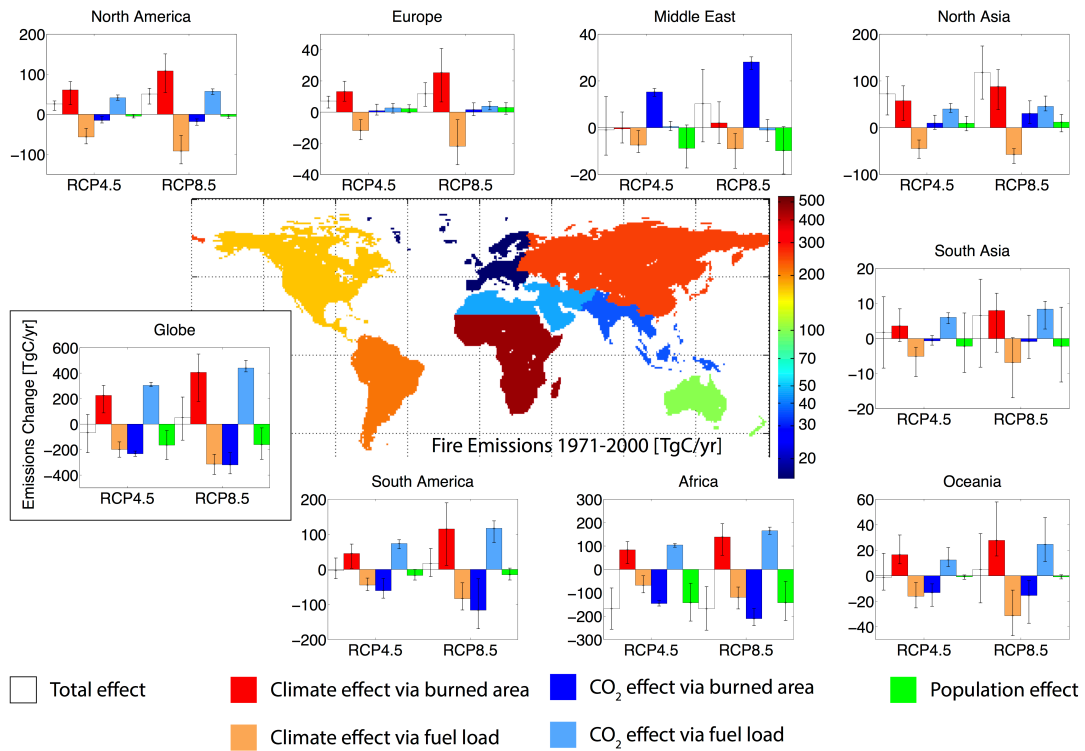
930



931

932 *Figure 4: Regional wildfire emissions during 1901-1930 for eight regions and global*
 933 *and regional changes, average 1971-2000 minus average 1901-1930, for ensemble*
 934 *mean (white/coloured bars) and range across ensemble comprising eight ESMs (error*
 935 *bars), in TgC/yr. The change in emissions is further subdivided into climate effect due*
 936 *to changes in burned area or changes in combusted fuel per burned area, effect of*
 937 *atmospheric CO₂ change due to changed burned are or fuel combustion, and*
 938 *population effect.*

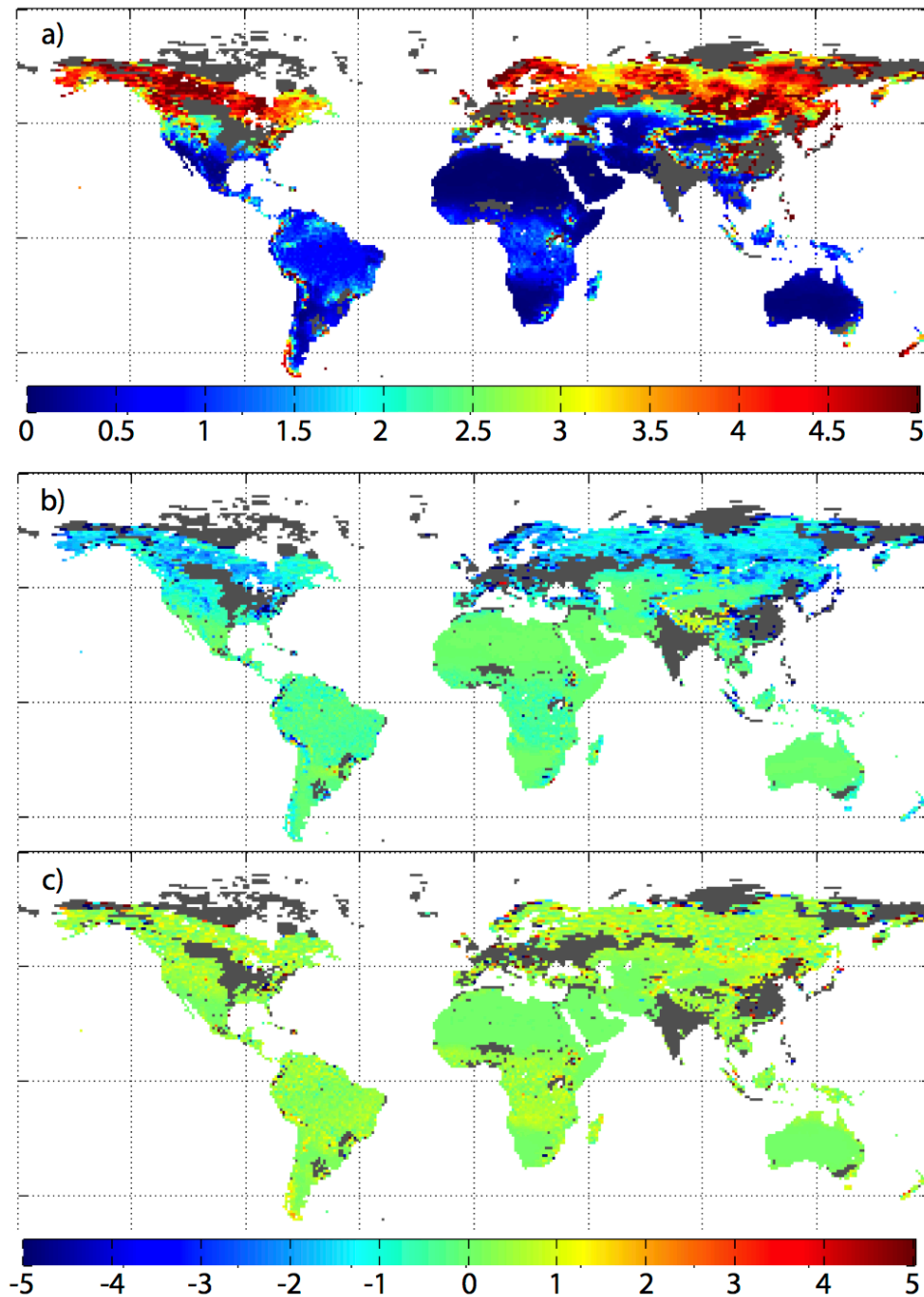
939



940

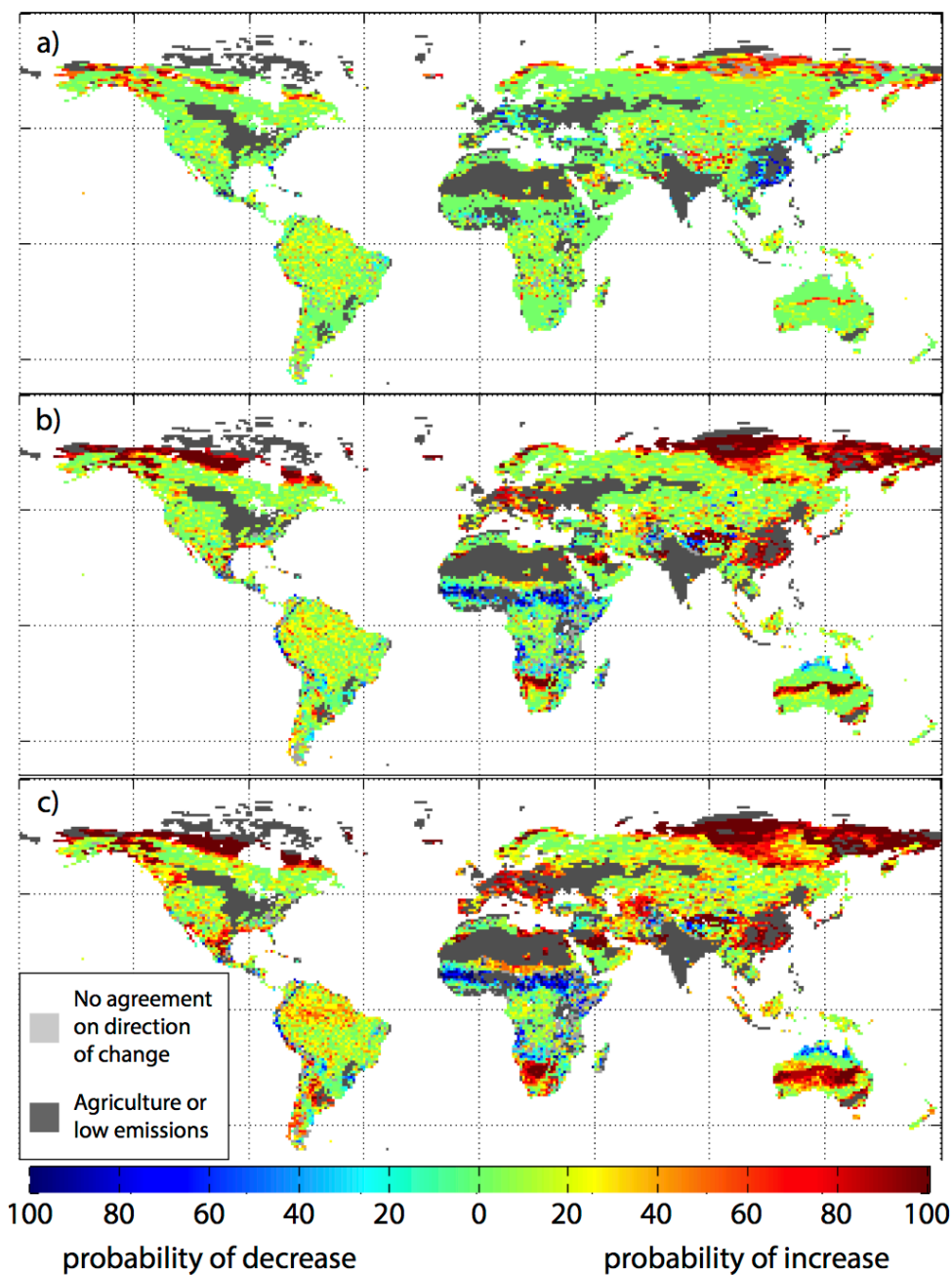
941 *Figure 5: As previous figure, but for average emissions during 1971-2000 and*
 942 *changes as 2071-2100 minus 1971-2000 averages, both differentiated between*
 943 *RCP4.5 and RCP8.5 climate scenarios. In this case, the ensemble is across eight*
 944 *ESMs times five population scenarios.*

945



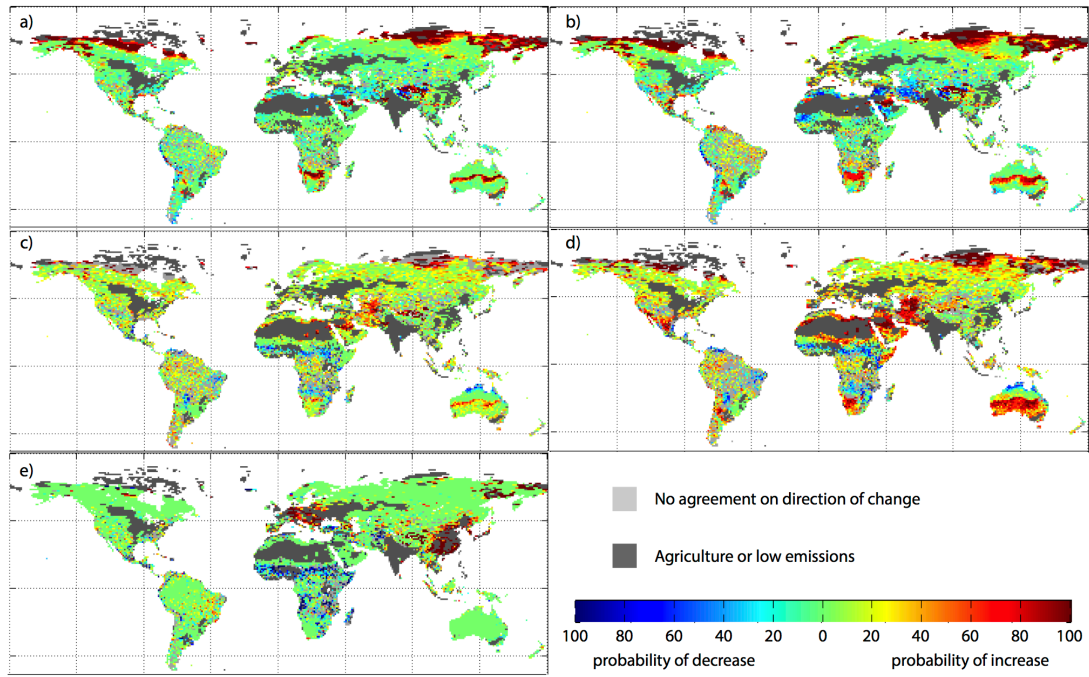
946

947 *Figure 6: Ensemble-mean combustible fuel load in kgC/m^2 and change due to climate*
 948 *and CO_2 effects. a) Average emissions 1971-2000; b) change from 1971-2000 to*
 949 *2071-2100 for RCP8.5 due to climate effect; c) same as b) but due to CO_2 effect. Grey*
 950 *areas have no fire or are excluded as dominated by agriculture. Combustible fuel*
 951 *load is the amount of carbon potentially emitted if a fire occurs.*



952

953 *Figure 7: Fraction of ensemble members with either a significant decrease or*
 954 *increase in wildfire emissions (positive or negative change by more than two standard*
 955 *deviations of the interannual variability of the initial period); Agricultural areas and*
 956 *areas with ensemble median emissions less than 10% of global median during 2071-*
 957 *2100 were excluded. a) Changes from 1901-1930 to 1971-2000; b) changes from*
 958 *1971-2000 to 2071-2100 for RCP4.5; c) as b) but for RCP8.5.*



959

960 *Figure 8: As previous figure, but for emissions changes due to single driving factors.*

961 *a, b) climate effect, c, d) CO₂ effect, e) population effect; a, c) RCP4.5, b, d) RCP8..*